Front. Earth Sci. 2016, 10(1): 117–125
DOI 10.1007/s11707-015-0512-9

RESEARCH ARTICLE

Long-range cross-correlation between urban impervious surfaces and land surface temperatures

Qin NIE (✉)[1], Jianhua XU[2], Wang MAN[1]

1 Department of Spatial Information Science and Engineering, Xiamen University of Technology, Xiamen 361024, China
2 The Research Center for East-West Cooperation in China, The Key Laboratory of GIScience, Ministry of Education of China, East China Normal University, Shanghai 200241, China

Abstract The thermal effect of urban impervious surfaces (UIS) is a complex problem. It is thus necessary to study the relationship between UIS and land surface temperatures (LST) using complexity science theory and methods. This paper investigates the long-range cross-correlation between UIS and LST with detrended cross-correlation analysis and multifractal detrended cross-correlation analysis, utilizing data from downtown Shanghai, China. UIS estimates were obtained from linear spectral mixture analysis, and LST was retrieved through application of the mono-window algorithm, using Landsat Thematic Mapper and Enhanced Thematic Mapper Plus data for 1997–2010. These results highlight a positive long-range cross-correlation between UIS and LST across People's Square in Shanghai. LST has a long memory for a certain spatial range of UIS values, such that a large increment in UIS is likely to be followed by a large increment in LST. While the multifractal long-range cross-correlation between UIS and LST was observed over a longer time period in the W–E direction (2002–2010) than in the N–S (2007–2010), these observed correlations show a weakening during the study period as urbanization increased.

Keywords urban impervious surface, land surface temperature, long-range cross-correlation, Shanghai

1 Introduction

Urbanization transforms land cover types from permeable land to anthropogenic urban impervious surface (UIS), causing a series of urban eco-environmental effects, with land surface temperature (LST) variations as one of the most important. UIS usually has higher solar radiation absorption, greater thermal conductivity, and a greater capacity for releasing daytime heat storage during the night. A well-documented consequence of this procedure is that UIS can affect urban LST by altering the sensible and latent heat fluxes that exist within and between the urban surface and boundary layers (Yang et al., 2003). Consequently, many studies have sought to analyze and understand the UIS–LST relationship (Yang and Liu, 2005; Weng et al., 2007; Xian et al., 2007; Xiao et al., 2007; Yuan and Bauer, 2007; Zhang et al., 2009). The warming effect of UIS on LST has been confirmed in various regions despite observed differences in their quantitative statistical relationship. Thus, a comprehensive understanding of the UIS–LST relationship is far from complete due to the complexity of the UIS thermal effect. While most studies have employed traditional statistical methods to investigate this relationship, the complexity of the urban environment warrants the implementation of complexity science theory and methods to fully explore this problem.

Complexity science, a new interdisciplinary science, has changed the perspective through which people understand issues. It breaks the traditional linear, balanced, simple paradigm of problem solving, and views a problem as a non-linear, non-equilibrium, complex adaptive system. The urban environment, for example, is a coupled natural–human–social–economic–geographical complex system. The spatial pattern of urban land use/cover and spatial differentiation of its thermal environment may seem fragmented and random, but they are geographical complexities with self-similar characteristics (Xu et al., 2001, 2003). Therefore, it is necessary to employ complexity theory and methodologies to study the UIS–LST relationship.

Fractal theory, one of the main means of understanding complexity, plays an important role in characterizing the

Received May 19, 2014; accepted December 10, 2014

E-mail: nieqinhongyi@163.com

UIS–LST relationship. It has been applied to measure the spatial complexity of UIS patterns (Xie et al., 2009; Liu et al., 2011; Liu et al., 2012), as well as to investigate urban LST. However, few studies have employed fractal theory to explore the UIS–LST relationship.

Detrended cross-correlation analysis (DCCA) and multifractal detrended cross-correlation analysis (MFDCCA) are employed for this fractal study of the UIS–LST relationship. DCCA, as outlined by Podobnik and Stanley (2008), is a generalization of detrended fluctuation analysis that is based on detrended covariance. It has been efficient in detecting long-range cross-correlations embedded in a data series exhibiting complex behavior (Wang et al., 2010; Vassoler and Zebende, 2012). The DCCA method can be generalized to MFDCCA to reveal the multifractal features of multi-dimensional cross-correlated series. The validity and potential utility of the MFDCCA method have been illustrated by Zhou (2008).

This paper analyses UIS and LST measurements from downtown Shanghai, China to: (i) investigate the long-range cross-correlations between the spatial patterns of UIS and LST using DCCA; and (ii) reveal the multifractal features of the cross-correlations between UIS and LST. UIS is first estimated from Landsat Thematic Mapper (TM) and Enhanced Thematic Mapper Plus (ETM+) data during 1997–2010 by using linear spectral mixture analysis (LSMA). The mono-window algorithm is applied to retrieve LST data. Two transects are then drawn (W–E and N–S profiles), and the data series of UIS and LST are extracted. Finally, DCCA and MFDCCA are employed to analyze the cross-correlations between UIS and LST.

2 Data and methods

2.1 Study area and data

We selected the downtown area of Shanghai, China as our study area, focusing within the outer ring road of the city (Fig. 1). As the largest economic center of China, Shanghai has experienced an accelerated urbanization rate (the ratio of urban population in total population), increasing from 59% during the economic reform of 1978 to 86% in 2007 (Yue et al., 2012). As a result, the land cover has undergone significant change. Most of the natural land cover has been converted to anthropogenic UIS, especially within the study area. Urban planning has matured since the development of Metropolitan Shanghai during the early 1990s, but several decision-making factors have encouraged Shanghai to develop more rapidly than other cities in China (Yue et al., 2007). Detection of the cross-correlations between UIS and LST could possibly contribute to urban development in the future. People's Square, one of the most well-known landmarks in Shanghai, is an important political, economic, and tourism center. The W–E and N–S profiles across People's Square are the two critical axes of urban development. This paper extracts UIS and LST data along both profiles to investigate the long-

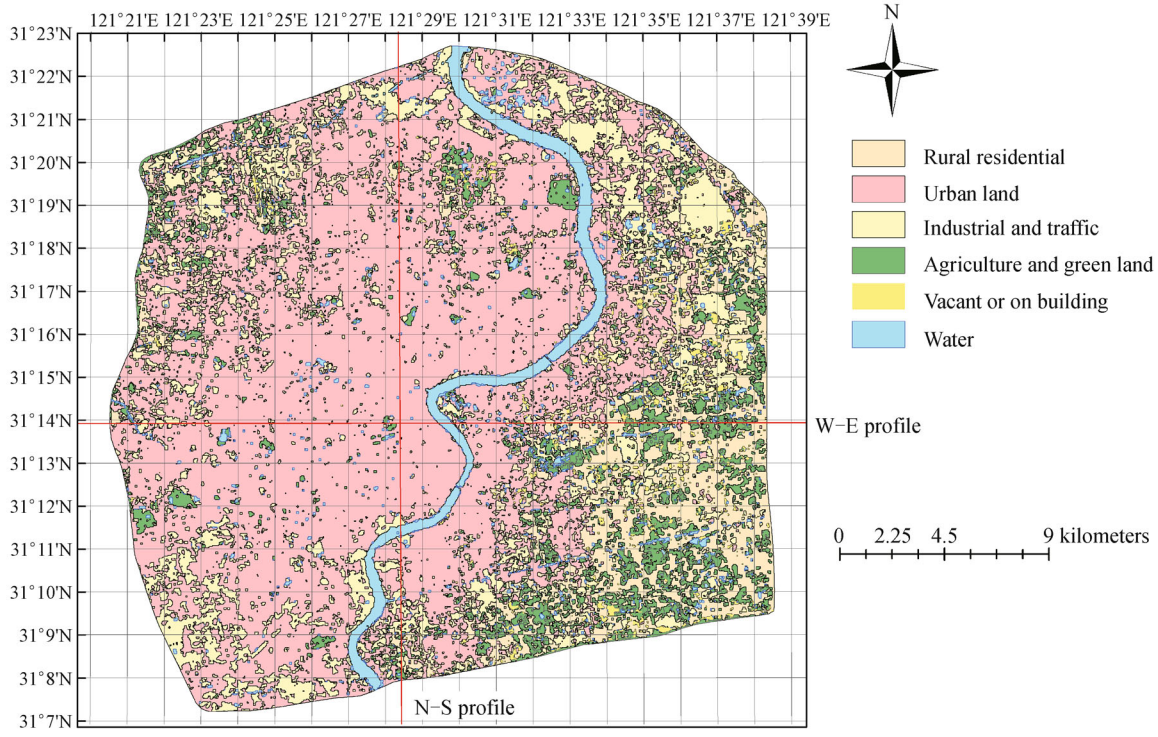

Fig. 1 Map of the study area.

range cross-correlations between their spatial patterns.

To avoid seasonal influence on the relationship between UIS and LST as much as possible, spring and autumn data have been used for this study. Four cloud-free TM/ETM+ images, acquired on 11 April 1997, 27 November 2002, 2 February 2007, and 9 November 2010, served as the primary data sources for mapping UIS and LST in the study area. All images were registered to 1:10,000 topographic maps of Shanghai. The images were then further rectified to a Shanghai coordinate system (a modified Transverse Mercator coordinate system). The resultant root mean square (RMS) values were found to be less than 0.5 pixels.

2.2 Estimation of UIS

UIS was estimated by LSMA. Based on Ridd's (1995) vegetation-impervious surface-soil (V-I-S) model, the spectrum, measured by a sensor, is a linear combination of the spectra of all components (endmembers) within a pixel. A typical LSMA model can be expressed as follows (Small, 2001):

$$R_i = \sum_{k=1}^{n} f_k R_{ik} + ER_i, \tag{1}$$

where i is the number of spectral bands, k is the number of endmembers, R_i is the spectral reflectance of band i containing all endmembers, f_k is the proportion of endmember k within the pixel, R_{ik} is the known spectral reflectance of endmember k within the pixel on band i, and ER_i is the error for band i. In this study, $k = 3$, and includes vegetation (trees and grass), high-albedo surfaces (metal structures, new concrete surfaces, sand, and some compound materials), and low-albedo surfaces (old concrete surfaces, cyan tiles, and asphalt). A sum of the high-albedo and low-albedo fractions was applied to determine UIS.

A constrained least-squares solution was used in this research, assuming that the following two conditions are simultaneously satisfied (Small, 2001):

$$\sum_{k=1}^{n} f_k = 1 \text{ and } 0 \leqslant f_k \leqslant 1. \tag{2}$$

Root Mean Square (RMS) error images were used to determine the overall error of all the endmember abundance values for each pixel. A lower RMS error of the abundance images is desired, where

$$\text{RMS} = \sqrt{\sum_{i=1}^{m} ER_i^2 / m}. \tag{3}$$

The accuracy assessment was conducted by the RMS image which appears as noise and determines the overall error of all of the endmember abundance values for each pixel. The areas with a high RMS error indicate low accuracy of spectral unmixing. In the 1997 example (Fig. 2), the majority of the pixels possess RMS error values less than 0.015. The spatially distributed image of the RMS error (Fig. 2) indicates that UIS tends to be overestimated around the outer ring road. When comparing UIS with the corresponding aerial image, these regions correlate to high-albedo features, such as the Shanghai Stadium and Hongkou Stadium. The overestimated UIS may be due to the building materials of these high-albedo features. For each of the other study years, the mean RMS error was less than 0.02, which suggests a generally good fit.

2.3 LST computation

LST data were retrieved using the procedure described by Artis and Carnahan (1982). The digital number (DN) of Landsat thermal band was first converted to spectral radiance (L_λ) according to the following equation:

$$L_\lambda = gain \times \text{DN} + offset, \tag{4}$$

where L_λ is the sensor radiance, *gain* is the slope of the radiance/DN conversion function, and *offset* is the intercept of the radiance/DN conversion function. The *gain* and *offset* values are supplied in the metadata

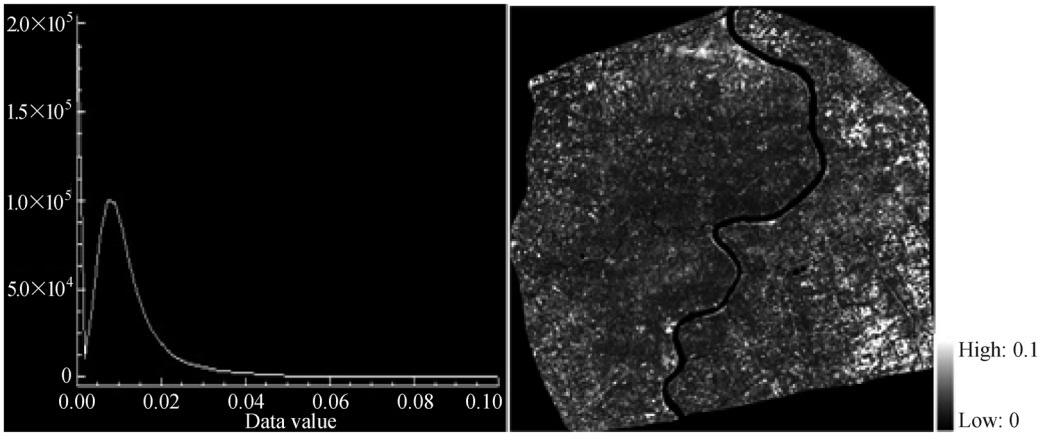

Fig. 2 The RMS frequency distribution and spatial image.

accompanying each TM/ETM+ image.

The temperature values of a black body were then derived using the inverse of the Planck function:

$$T_B = \frac{K_2}{\ln\left(\frac{K_1}{L_\lambda}+1\right)}, \quad (5)$$

where T_B is the effective at-satellite temperature (in Kelvin), L_λ is the spectral radiance, and K_1 and K_2 are calibration constants, which are supplied from the metadata associated with the Landsat images. For the TM data, K_1= 607.76 and K_2= 1,260.56. For the ETM+ data, K_1= 666.09 and K_2= 1,282.71.

The LST can then be obtained by applying corrections for emissivity (ε) on T_B:

$$\mathrm{LST} = \frac{T_B}{1+(\lambda \times T_B/\rho)\ln\varepsilon}, \quad (6)$$

where λ is the wavelength of the emitted radiance (11.5 μm), $\rho = h \times c/\sigma$, h is Planck's constant (6.626×10^{-34} Js), σ is the Boltzmann constant (1.38×10^{-23} J/K), c is the velocity of light (2.998×10^8 m/s), and ε is the land surface thermal emissivity. We used the normalized difference vegetation index (NDVI) threshold method to obtain ε. Based on Van de Griend and Owe (1993), emissivity (ε) is 0.9925 for water surface. For other types of land cover, it can be determined as:

$$\begin{cases} \varepsilon = 1.0094 + 0.047 \times \ln(\mathrm{NDVI}) & \mathrm{NDVI} > 0.157 \\ \varepsilon = 0.923 & \mathrm{NDVI} \leqslant 0.157 \end{cases}. \quad (7)$$

The LST values derived above are reliable. First, in the conversion from DN values into spectral radiance, the radiation correction formula provided by the Landsat user manual was applied. These results are also reliable. During the conversion from spectral radiance into the effective at-satellite temperature, the calibration coefficients are also supplied by the metadata of Landsat images. Finally, the emissivity corrected surface temperature was computed based on the empirical formula of Van de Griend and Owe (1993) and Gong et al. (2005), and has also been demonstrated by many other researchers.

2.4 DCCA

2.4.1 DCCA

We investigated the long-range cross-correlations between the spatial patterns of UIS and LST using DCCA. For two series of length N, $\{x_i\}$ and $\{y_i\}$, the zero-mean series is obtained as:

$$x_i = x_i - \overline{x},\ y_i = y_i - \overline{y},\ \overline{x} = \sum_{i=1}^{N} x_i,\ \overline{y} = \sum_{i=1}^{N} y_i, \quad (8)$$

where $\overline{x}$ and $\overline{y}$ are the mean values of series x_i and y_i, respectively.

The integrated series is computed as:

$$R_k = \sum_{i=1}^{k} x_i,\ R'_k = \sum_{i=1}^{k} y_i,\ k = 1,2,...,N. \quad (9)$$

Selecting scale s, the integrated series is divided into non-overlapping boxes, each containing s values. The amount of boxes is: $N_s = \mathrm{int}(N/s)$. Because N may not be divisible by s, the end points of series may not enter into the operation. To solve this problem, the division process is repeated from the end of the data sequence; therefore 2 N_s small boxes are obtained.

For the box v, the local trend $\tilde{R}_{k,v}$ and $\tilde{R}'_{k,v}$ is defined by a linear least-squares fit. Next, the covariance of the residuals in the box v is obtained:

$$f^2(s,v) = \frac{1}{s}\sum_{k=1}^{s}\left(R_k - \tilde{R}_{k,v}\right)\left(R'_k - \tilde{R}'_{k,v}\right). \quad (10)$$

Finally, the detrended covariance function is obtained by summing over all non-overlapping boxes of size s:

$$F^2(s) = \frac{1}{2N_s}\sum_{v=1}^{2N_s} f^2(s,v). \quad (11)$$

In general, the double logarithm linear relationship is found:

$$F^2(s) \sim s^\lambda, \quad (12)$$

where λ= 0.5 corresponds to the Gaussian white noise; that is to say that there is no cross-correlation between the two series. $\lambda \neq 0.5$ indicates that the two series are not isolated and are long-range cross-correlations. Specifically, if $0.5 < \lambda < 1$, the positive long-range cross-correlation is present; if $0 < \lambda < 0.5$, the negative power-law long-range cross-correlation is present. λ= 1 corresponds to *1/f* behavior. $\lambda > 1$ indicates the existence of long-range cross-correlations, but not the form of power-law cross-correlation. $\lambda > 1.5$ corresponds to Brownian noise.

2.4.2 MFDCCA

MFDCCA was used to reveal the multifractal features of the cross-correlations between UIS and LST. When MFDCCA is implemented, the q^{th} order detrended covariance for each box can be calculated as follows:

$$F_{xy}(q,s) = \left[\frac{1}{m}\sum_{v=1}^{m} F_v(s)^{q/2}\right]^{1/q}, \quad (13)$$

where $q \neq 0$ and

$$F_{xy}(0,s) = \exp\left[\frac{1}{2m}\sum_{v=1}^{m}\ln F_v(s)\right]. \quad (14)$$

We then expect the following scaling relation

$$F_{xy}(q,s) \sim s^{h_{xy}(q)}, \quad (15)$$

when $x = y$, the above method reduces to the classic multifractal detrended fluctuation analysis.

The mass exponent $\tau(q)$ can be obtained:

$$\tau_{xy}(q) = qh_{xy}(q) - 1. \quad (16)$$

If $\tau_{xy}(q)$, and q is nonlinear, the cross-correlation is multifractal. The multifractal spectrum can be obtained:

$$\alpha = h_{xy}(q) + qh'_{xy}(q),\ f_{xy}(\alpha) = q\left(\alpha - h_{xy}(q)\right) + 1. \quad (17)$$

The strength of multifractal can be measured:

$$\Delta\alpha = \alpha_{\max} - \alpha_{\min}. \quad (18)$$

The greater the $\Delta\alpha$ value, the stronger the multifractal.

3 Results

This paper extracts UIS and LST data along both profiles for four time periods (1997, 2002, 2007, and 2010). The long-range cross-correlations between UIS and LST are explored using DCCA and MFDCCA.

3.1 Long-range cross-correlation between UIS and LST

The spatial patterns of UIS and LST along the N–S profile are shown by log–log plots of the detrended covariance $F^2(s)$ versus scale s from 1997 to 2010 (Fig. 3). Scale-free intervals are identified in these plots, where a simple linear fit to the data exists. Of note, the scaling exponent λ, which is the slope for each linear fit, is greater than 0.5 for the four examined years. This indicates that the spatial patterns of UIS and LST on the N–S profile exhibit positive long-range cross-correlations. Long-range cross-correlations between UIS and LST imply that LST has a "long memory" for a certain spatial range of UIS values, suggesting that a large increment in UIS fraction is likely to be followed by a large increment in LST, and vice versa. Furthermore, a power-law behavior was observed for the cross-correlations between UIS and LST in 2002, 2007, and 2010, because $0.5 < \lambda < 1$. The 1997 cross-correlations, however, do not exhibit a power-law-type behavior, since $\lambda = 1.122$.

The temporal trend in λ shows that the long-range cross-correlation function between UIS and LST exhibits a power-law decay from 2002 to 2010. This signifies that the fluctuations between UIS and LST are positively cross-correlated in a power-law fashion. This long-range cross-

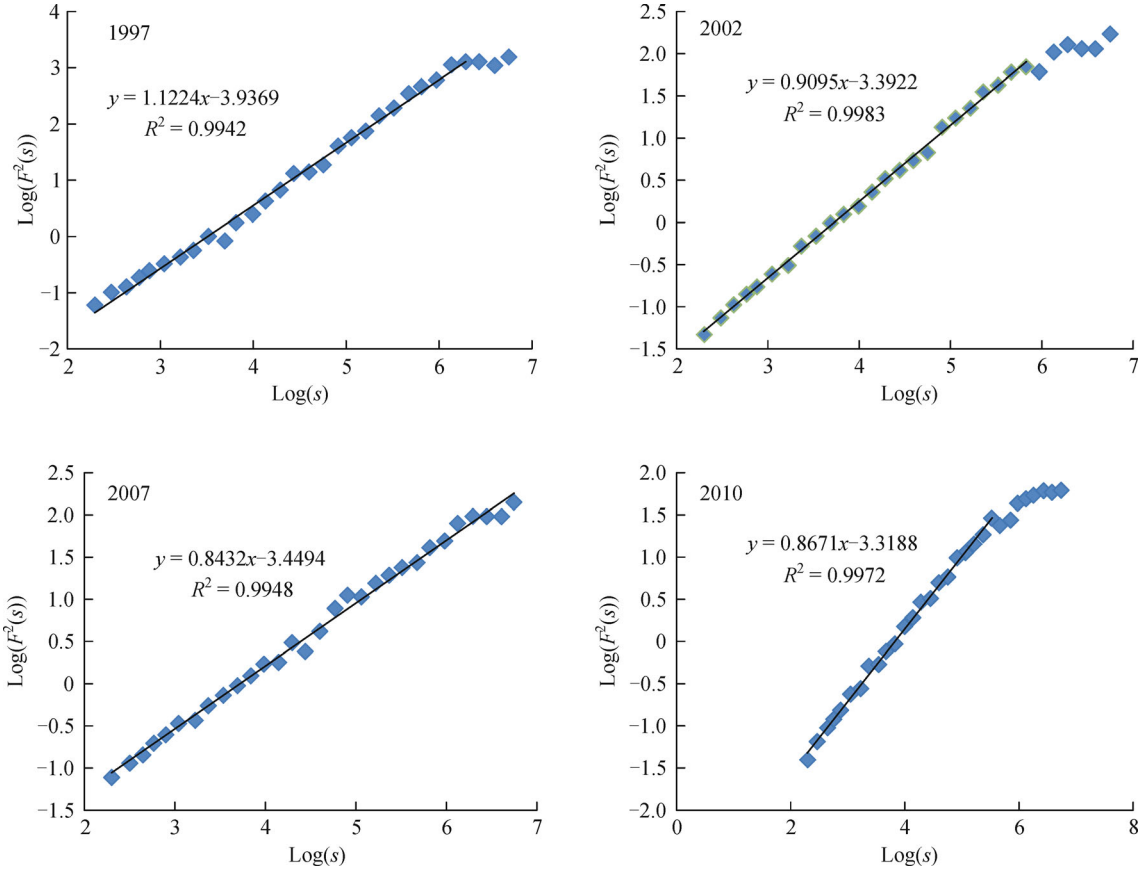

Fig. 3 Log–log plots of the detrended fluctuations $F^2(s)$ versus scale s for the N–S profile.

correlation refers to the "long memory" or cross-correlation between UIS and LST. For example, an increase in UIS fraction is followed by an increase in LST at a different spatial scale. This finding suggests that the cross-correlations between the fluctuations of UIS and LST do not obey the classical Markov-type stochastic behavior (exponential decrease with space), but rather decay in a slower fashion. According to λ, the cross-correlation between the spatial patterns of UIS and LST decreases from 1997 to 2010, indicating that the influence of UIS on LST decreases significantly during the study period.

Two scale-free intervals were observed in the log–log plots of the W–E profile for each examined year (Fig. 4). For each scale-free interval, we have $\lambda > 0.5$, highlighting a positive long-range cross-correlation between UIS and LST. In the first scale-free interval, we have $0.5 < \lambda < 1$ in 1997 and 2002, suggesting a power-law long-range cross-correlation between UIS and LST. In addition, we have $\lambda = 1 \pm 0.01$ in 2007 and 2010, exhibiting a $1/f$ behavior. In the second scale-free interval, we have $1 < \lambda < 1.5$ in 1997 and 2002, suggesting that the cross-correlations do not obey a power-law-type behavior; however, we have $0.5 < \lambda < 1$ in 2007 and 2010, indicating a long-range cross-correlation in a power-law fashion.

The W–E profile is divided into Puxi and Pudong by the Huangpu River. The Puxi section is the old city, whereas the Pudong section is mostly farmland. The first scale-free interval is located in Puxi, highlighting an increased long-range cross-correlation between 1997 and 2010; the second scale-free interval is located in Pudong, pointing to a reduced cross-correlation over the same time period (Fig. 4).

As indicated from the above analysis, it can be concluded that the long-range cross-correlation between UIS and LST decreases with increasing urbanization. The N–S profile highlights a decreasing long-range cross-correlation from 1997 to 2010 that displays a slower decaying power-law behavior from 2002 to 2007. A similar trend is observed for the Pudong section of the W–E profile, where urbanization appears to influence the decreasing cross-correlation in this area during the study period. The highly urbanized Puxi section, where limited cross-correlation variability is observed, exhibits an approximate $1/f$ behavior.

3.2 Multifractal nature of long-range cross-correlation between UIS and LST

MFDCCA was used to reveal the multifractal features of the cross-correlated UIS and LST. The long-range cross-correlations between UIS and LST exhibit a multifractal nature, as highlighted by the nonlinear relationship between the mass exponent $\tau_{xy}(q)$ and the order q across downtown Shanghai in 2007 and 2010, and also in 2002 for the W–E profile (Figs. 5 and 6). In 1997, $\tau_{xy}(q)$ exhibits a linear relationship with q, indicating no multifractal long-range cross-correlation between the UIS and LST. A single scaling exponent can thus characterize the long-range cross-correlation at the beginning of the study period.

The multifractal parameter $\Delta\alpha$ was calculated to describe

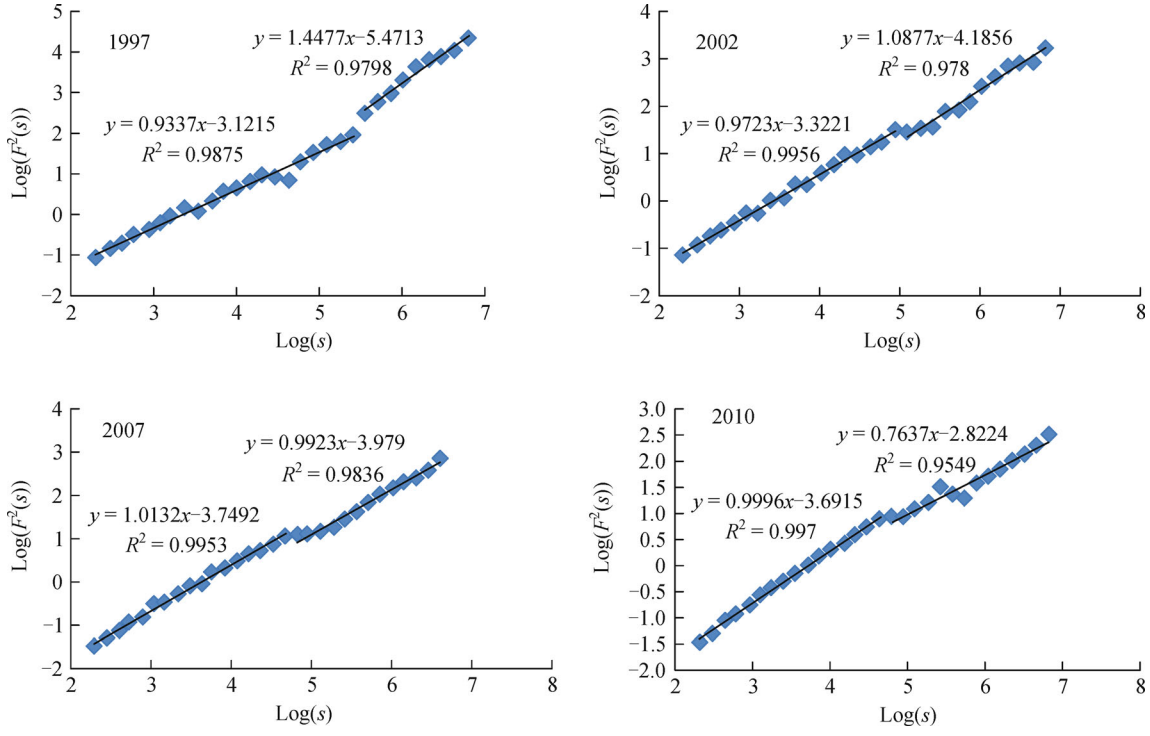

Fig. 4 Log–log plots of the detrended fluctuations $F^2(s)$ versus scale s for the W–E profile.

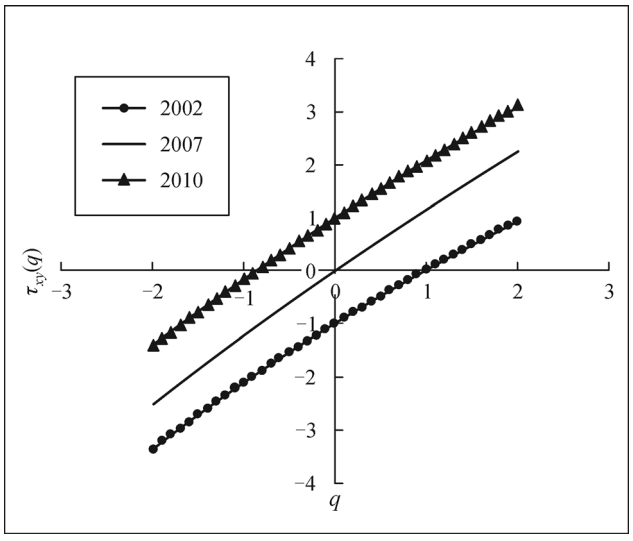

Fig. 5 Dependence of the mass exponent function $\tau_{xy}(q)$ with respect to the order q on the W–E profile. The plots for 2007 and 2010 are shifted upward by 1 and 2 units for clarity, respectively.

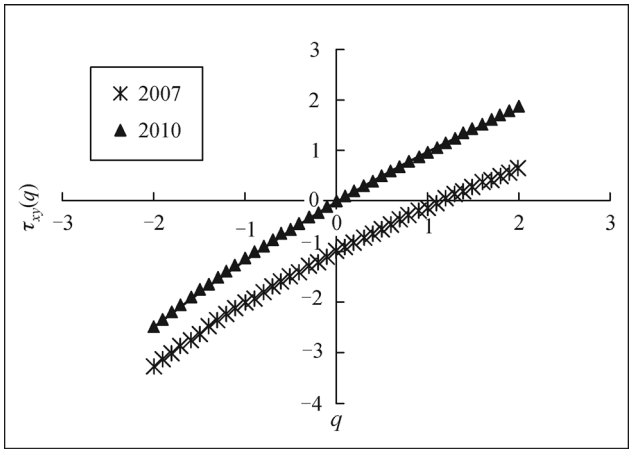

Fig. 6 Dependence of the mass exponent function $\tau_{xy}(q)$ with respect to the order q on the N–S profile. The plots for 2010 are shifted upward by 1 unit for clarity.

the multifractal nature (Table 1) of the singularity exponent α and the multifractal spectrum $f(\alpha)$ (Figs. 7 and 8). The minimum and maximum probability measures ($\alpha_{\max}$ and $\alpha_{\min}$, respectively) can be used to describe the range of probability measures for a given cross-correlation, with a width of $\Delta\alpha = \alpha_{\max} - \alpha_{\min}$. The greater the value, the wider the probability distribution and the more irregular the cross-correlation. The W–E profile exhibits a decrease from 2002 to 2010, indicating a decrease in the multifractal nature of the long-range cross-correlation between UIS fraction and LST, resulting in an increase in the uniform probability distribution. A slight decrease in $\Delta\alpha$ is observed from 2007 to 2010 for the N–S profile, indicating that its multifractal nature and the probability distribution

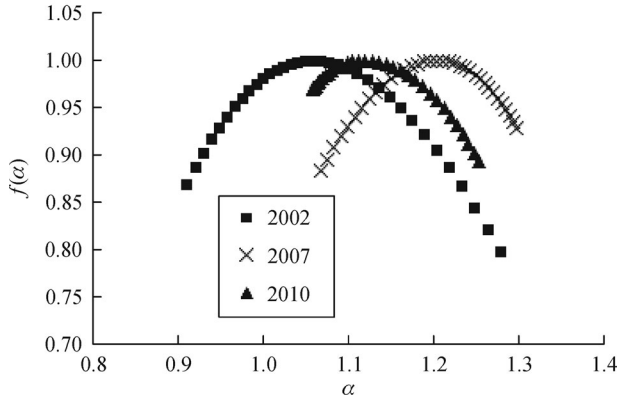

Fig. 7 Multifractal spectra of the long-range cross-correlation on the W–E profile.

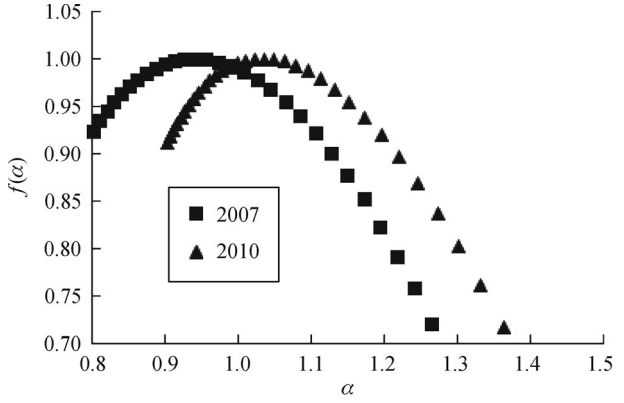

Fig. 8 Multifractal spectra of the long-range cross-correlation on the N–S profile.

show minimal changes over time. However, the multifractal nature of the N–S profile is stronger than that of the W–E profile. From the above analysis, the decreasing multifractality on both profiles further indicates that the UIS has a decreasing influence on LST with the increasing urbanization of Shanghai city.

4 Discussion and conclusions

4.1 Discussion

4.1.1 Long-range cross-correlation between UIS and LST

This paper focuses on the quantitative relationship between LST and UIS. Plenty of literature is available on this topic, but few studies are from the point of view of the long-range cross-correlation. This study indicates that the influence of UIS on LST exist fractal characteristic, as indicated by the positive long-range cross-correlations.

That is to say that LST has a "long memory" for a certain

Table 1 The parameter of multifractal spectra

Profile	Year	$\Delta\alpha$
W−E profile	2002	0.37
	2007	0.23
	2010	0.19
N−S profile	2007	0.534
	2010	0.527

spatial range of UIS values. A large increment in UIS fraction is followed by a large increment in LST values of a certain spatial scale, and vice versa.

A decreasing long-range cross-correlation between UIS and LST is found over time. The increasing urbanization influences the decreasing cross-correlation. Urban planning has matured since the development of Metropolitan Shanghai during the early 1990s, and improved decision-making factors have encouraged more rational development than observed in other cities in China (Yue et al., 2007). Rational urban planning can mitigate the impact of UIS on LST, resulting in a decreased cross-correlation between UIS and LST.

The influence of UIS on LST has increased in complexity with urbanization. At the beginning of the study period, a single scaling exponent can characterize the long-range cross-correlation. However, with increasing urbanization, the multifractal long-range cross-correlation between the UIS and LST is present. Thus, a series of scaling exponents are necessary to describe the long-range cross-correlation, which becomes increasingly complex. Furthermore, it can be seen how the multifractal cross-correlation between UIS and LST evolves with urbanization. As indicated by the decreasing values, the probability distribution of the cross-correlation becomes gradually uniform over time, which is a result of urbanization. Shanghai developed the new urban master plan in 2000 to promote balanced development between the cities in the Yangtze River Delta region. Large-scale residential buildings, satellite cities, industrial parks, and various kinds of functional zones have since been built in the study area. Meanwhile, a significantly improved transportation network system has been developed to meet the increasing needs of the greater urban area. As a result, the spatial heterogeneity of the UIS spatial pattern has been weakened. Therefore, the cross-correlation between UIS and LST in the study area mirrors the government policy and economic development.

4.1.2 Application of the DCCA method to the UIS-LST relationship

The UIS spatial pattern and the spatial differentiation of its thermal environment exhibit complex behavior, such as self-similarity, thus we can apply new strategies for its analysis. From this point of view, one of the most frequently cited methods for analyzing a data series of complex problems is the detrended fluctuation analysis (DFA). This method provides a relationship between $F_{\mathrm{DFA}}(n)$ (root mean square fluctuation) and the scale n. The DFA method has proven to be very efficient for detecting long-range auto-correlations embedded in a data series and also for avoiding spurious detection of apparent long-range auto-correlations. This has been shown to be true in a great number of applications and citations. However, for two simultaneously recorded series, $\{x_i\}$ and $\{y_i\}$, the analysis of cross-correlation can be applied. The DCCA method is a generalization of the DFA method and is based on detrended covariance. It has been successfully applied in many situations and has yielded significant results (Podobnik and Stanley, 2008; Podobnik et al., 2009; Vassoler and Zebende, 2012).

However, as revealed in other literature, obtaining a reliable value of the scaling exponent λ by applying DCCA/MFDCCA is not an easy calculation. The method applies a box counting method to obtain the scaling exponent, which partitions the study space into non-overlapping boxes to construct samples with multiple scales. The number of samples at a given scale is restricted by the size of the partitioning space and data resolution, which is usually a main factor for influencing statistical estimation. This is more important in MFDCCA, especially for negative q moments. To avoid the problem, some improved methods have been proposed, such as the gliding box method which constructs samples by gliding a box of certain size (α) over a grid map in all possible directions (Grau et al., 2006). Nevertheless, in order to examine the patterns of spatial distribution of urban built-up elements, the box counting method is an excellent approach for evaluating fractal dimension, as Chen (2013) suggests. This research indicated that application of the DCCA method to the UIS-LST relationship yielded significant results. It was determined that, based on the comparison of results from different algorithms, such as the gliding box algorithm, including numerical differences and standard error values, future discussions are essential.

4.2 Conclusions

This paper employed TM/ETM+ data to estimate UIS and LST during 1997–2010 for downtown Shanghai, China. The fractal and multifractal characteristics of the correlation between UIS and LST were then investigated. Positive long-range cross-correlations between UIS and LST were observed across People's Square. These cross-correlations indicate that LST has a long memory for a certain spatial range of UIS values. A large increment in UIS fraction is more likely to be followed by a large increment in LST. Furthermore, the long-range cross-correlations exhibit a power-law behavior on the N–S profile from 2002 to 2010. Two scale-free intervals were found on the W–E profile. In

the first scale-free interval, UIS and LST exhibit a power-law long-range cross-correlation in 1997 and 2002 that evolves to a $1/f$ behavior in 2007 and 2010. In the second scale-free interval, the long-range cross-correlation evolves from a non-power-law behavior in 1997 and 2002 to a power-law behavior in 2007 and 2010. This long-range cross-correlation between UIS and LST exhibits a multifractal nature across downtown Shanghai in 2007 and 2010, as well as in 2002 for the W–E profile. The decrease in multifractal strength during the study period suggests that UIS fraction has a decreased influence on LST with the growing urbanization of Shanghai.

Acknowledgements This work was supported by the National Natural Science Foundation of China (Grant Nos. 41102224 and 41130525).

References

Artis D A, Carnahan W H (1982). Survey of emissivity variability in thermography of urban areas. Remote Sens Environ, 12(4): 313–329

Chen Y G (2013). Fractal analytical approach of urban form based on spatial correlation function. Chaos Solitons Fractals, 49: 47–60

Gong A D, Jiang Z X, Li J, Chen Y H, Hu H L (2005). Urban land surface temperature retrieval based on landsat TM remote sensing images in Beijing. Remote Sensing Information, (3): 18–20

Grau J, Méndez V, Tarquis A M, Díaz M C, Saa A (2006). Comparison of gliding box and box-counting methods in soil image analysis. Geoderma, 134(3–4): 349–359

Liu Z H, Wang Y L, Peng J (2012). Quantifying spatiotemporal patterns dynamics of impervious surface in Shenzhen. Geogrpahical Research, 31: 1535–1545 (in Chinese)

Liu Z H, Wang Y L, Peng J, Xie M M, Li Y (2011). Using ISA to analyze the spatial pattern of urban land cover change: a case study in Shenzhen. Acta Geogr Sin, 66(7): 961–971

Podobnik B, Grosse I, Horvati'c D, Ilic S, Ivanov P Ch, Stanley H E (2009). Quantifying cross-correlations using local and global detrending approaches. Eur Phys J B, 71(2): 243–250

Podobnik B, Stanley H E (2008). Detrended cross-correlation analysis: a new method for analyzing two nonstationary time series. Phys Rev Lett, 100(8): 084102

Ridd M K (1995). Exploring a V-I-S (vegetation-impervious surface-soil) model for urban ecosystem analysis through remote sensing: comparative anatomy for cities. Int J Remote Sens, 16(12): 2165–2185

Small C (2001). Estimation of urban vegetation abundance by spectral mixture analysis. Int J Remote Sens, 22(7): 1305–1334

Van de Griend A A, Owe M (1993). On the relationship between thermal emissivity an d the normalized diference vegetation index for nature surfaces. Int J Remote Sens, 14(6): 1119–1131

Vassoler R T, Zebende G F (2012). DCCA cross-correlation coefficient apply in time series of air temperature and air relative humidity. Physica A: Statistical Mechanics and its Applications, 391: 2438–2443

Wang Y, Wei Y, Wu C (2010). Cross-correlations between Chinese A-share and B-share markets. Physica A: Statistical Mechanics and its Applications, 389: 5468–5478

Weng Q, Liu H, Lu D (2007). Assessing the effects of land use and land cover patterns on thermal conditions using land scape metrics in city of Indianapolis, United States. Urban Ecosyst, 10(2): 203–219

Xian G, Crane M, Su J (2007). An analysis of urban development and its environmental impact on the Tampa Bay watershed. J Environ Manage, 85(4): 965–976

Xiao R B, Ouyang Z Y, Zheng H, Li E F, Schienke E W, Wang X K (2007). Spatial pattern of impervious surfaces and their impacts on land surface temperature in Beijing, China. J Environ Sci (China), 19 (2): 250–256

Xie M M, Wang Y L, Li G C (2009). Spatial variation of impervious surface area and vegetation cover based on SubPixel Model in Shenzhen. Resources Science, 31: 257–264 (in Chinese)

Xu J H, Ai N S, Chen Y, Mei A X, Liao H J (2003). Quantitative analysis and fractal modeling on the mosaic structure of landscape in the central area of Shanghai metropolis. Chin Geogr Sci, 13(3): 199–206

Xu J H, Lu Y, Ai N S, Yue W Z (2001). A study on landscape mosaic structure in urban-rural area in Northwest of China with RS and GIS. Chin Geogr Sci, 11(4): 366–376

Yang L, Huang C, Homer C G, Wylie B K, Coan M J (2003). An approach for mapping large-area impervious surfaces: synergistic use of Landsat-7 ETM+ and high spatial resolution imagery. Can J Rem Sens, 29(2): 230–240

Yang X, Liu Z (2005). Use of satellite-derived landscape imperviousness index to characterize urban spatial growth. Comput Environ Urban Syst, 29(5): 524–540

Yuan F, Bauer M E (2007). Comparison of impervious surface area and normalized difference vegetation index as indicators of surface urban heat island effects in Landsat imagery. Remote Sens Environ, 106(3): 375–386

Yue W, Liu Y, Fan P, Ye X, Wu C (2012). Assessing spatial pattern of urban thermal environment in Shanghai, China. Stochastic Environ Res Risk Assess, 26(7): 899–911

Yue W, Xu J, Tan W, Xu L (2007). The relationship between land surface temperature and NDVI with remote sensing: application to Shanghai Landsat 7 ETM+ data. Int J Remote Sens, 28(15): 3205–3226

Zhang Y, Odeh I O A, Han C (2009). Bi-temporal characterization of land surface temperature in relation to impervious surface area, NDVI and NDBI, using a sub-pixel image analysis. Int J Appl Earth Obs Geoinf, 11(4): 256–264

Zhou W X (2008). Multifractal detrended cross-correlation analysis for two nonstationary signals. Phys Rev E Stat Nonlin Soft Matter Phys, 77(6): 066211